The Journal of Engineering

The 9th International Conference on Power Electronics, Machines and Drives (PEMD 2018)

IET Journals
The Institution of Engineering and Technology

Rapid sizing concept of interior permanent magnet machine for traction applications

eISSN 2051-3305
Received on 25th June 2018
Accepted on 30th July 2018
doi: 10.1049/joe.2018.8169
www.ietdl.org

Khoa Dang Hoang[1] ✉, *Kais Atallah*[1]

[1]*Department of Electronic and Electrical Engineering, University of Sheffield, Mappin Street, Sheffield S1 3JD, UK*

✉ *E-mail: k.hoang@sheffield.ac.uk*

Abstract: This study presents a rapid sizing technique for interior permanent magnet (IPM) machine in traction application considering saturation effects. It is demonstrated that with limited computing resources, sizing, parameters considering saturation effects, and efficiency maps (loss maps) of an IPM machine can be generated within seconds with acceptable accuracy in comparison with finite element study and measurements. Thus, the proposed rapid sizing method is highly essential at the preliminary design stage of electric vehicle powertrains.

1 Introduction

Due to their high efficiencies, permanent magnet synchronous machines (PMSM) are widely employed for traction applications [1]. However, because of the relatively lower energy density of batteries directly affecting the vehicle range and cost, electric vehicle (EV) powertrains should be very carefully optimised and matched to the vehicle and its corresponding operating cycles. For traction application, interior permanent magnet (IPM) machine is often employed due to its high capability of field weakening operation [2]. Unfortunately, IPM machine is well known for its high non-linear characteristics that often require extensive finite element (FE) analysis for a specific geometry. Therefore, the development of a tool for the rapid sizing and generation of IPM machine non-linear characteristics together with its efficiencies (loss maps) is essential to facilitate the initial design stage of EV powertrains [3].

In this paper, a rapid sizing method for IPM machine considering electrical steel saturation effects is presented. It is noted that a similar technique can be applied for sizing of surface-mounted permanent magnet (SPM) machine. First, based on the EV specifications, maximum power and maximum speed required of the specific vehicle over a given driving cycle can be obtained. Under the assumption that the traction machine driving this EV may be often implemented with short-period overload up to two times and with operated speed three to five higher times of its base speed in the flux-weakening (FW) region, continuous rated torque and base speed of the required traction machine can be approximated. However, it is noted that the torque–speed characteristic can be also be defined by the powertrain developer. Then, the relevant optimum pole pair and stator slot number are selected. Based on the maximum achievable specifications of utilised materials (copper current density, electrical steel flux density, and air gap flux density) at this continuous rated torque and base speed operating point, dimensions of the studied IPM machine including stator stack length (L_{stk}), outer stator diameter (D_{os}), inner stator diameter (D_{is}), and outer rotor diameter (D_{or}) can be evaluated for maximum torque per machine volume achievement with a specific machine efficiency. From these obtained dimensions, stator geometries (slot depth, yoke depth, tooth width etc) can be determined to satisfy the selected air gap flux density. Then, the current limitation of the machine together with the stator winding turn number can be derived to satisfy the required electromagnetic torque. Using this turn number considering achievable current density associated with the cooling method, stator inductance and stator resistance can be computed. In addition, DC link voltage V_{dc} of the machine is often selected to balance machine voltage at base speed under peak torque demand. As traction machine in the EV will be driven via battery in the electric operating mode, there is often a current and voltage limitation associated with the employed battery pack. These values should be considered to finalise the maximum current I_{max} and DC link voltage V_{dc}. In the rotor side, magnet pole–arc angle value is selected to minimise total harmonic distortion of air gap flux density [1], whereas the iron bridge length is analysed to withstand its own centrifugal force and that of the inner magnets [4]. On the other hand, the magnet length is determined to achieve the required air gap flux density, ensure demagnetising protection, and maintain the saliency factor for the achievement of the required reluctance torque. Then, required magnet volume can be derived. After stator and rotor geometries of the studied IPM machine are defined, machine *dq*-axis inductances together with PM flux linkage considering saturation effects can be derived via iterating *B–H* curve of the employed electrical steel material [5]. Using these non-linear machine parameters, machine efficiency map together with relevant loss maps can be obtained [3]. In practice, with limited computing resources, all the aforementioned steps can be completed within seconds with acceptable accuracy compared with FE study and measurements.

2 Proposed sizing concept

The purpose of the proposed method is to rapidly generate sizing of an IPM traction machine with a torque–speed characteristic considering material saturation with reasonable accuracy.

2.1 Common dimension sizing

In this section, sizing of common dimensions for an IPM traction machine including inner stator diameter (D_{is}), outer stator diameter (D_{os}), and stator stack length (l_{stk}) is presented. Generally, these values should be selected for the traction machine to maintain a specific operating torque and speed range required over a specific driving cycle. According to [3], based on the specifications of an EV, the total tractive effort (F_{te}) and its components over a specific driving cycle can be derived as

$$\begin{aligned} & F_{te} = F_{rr} + F_{ad} + F_{rg} + F_{la} \\ \text{where} \quad & F_{rr} = \mu_{rr} m_v g \cos(\alpha) \\ & F_{ad} = \rho_{air} C_d A_f v^2/2 \\ & F_{rg} = m_v g \sin(\alpha); F_{la} = m_v a \end{aligned} \tag{1}$$

F_{rr}, F_{ad}, F_{rg}, and F_{la} are the rolling resistance force, aerodynamic force, road grade force, and linear acceleration force, respectively; μ_{rr} is the rolling resistance coefficient; m_v is the vehicle mass; g is

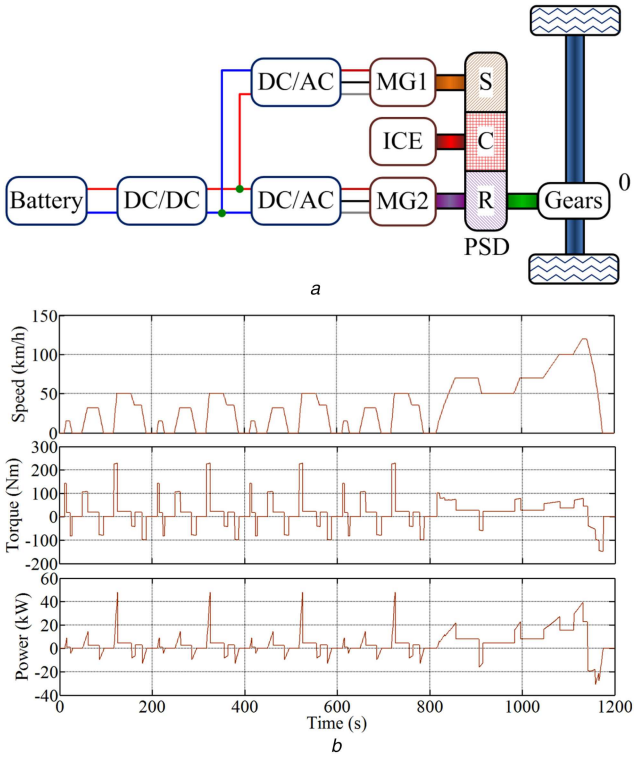

Fig. 1 *Toyota Prius 2004 specifications [3].*
(a) Powertrain. ***(b)*** Relevant torque and power demand over NEDC

the gravitational acceleration; p_{air} is the air density; C_d is the drag coefficient; A_f is the front area of the vehicle; v is the vehicle speed; and α is the road angle.

The total tractive effort in (1) must be balanced by the generated traction machine torque T_e and relevant power demand P_{de} applied to the EV wheels shown as

$$T_\Sigma = r_{wheel}F_{te} = \eta_g n_g T_e;\ P_{de} = \omega_m T_e \tag{2}$$

where r_{wheel} is the wheel radius; n_g is the gear ratio; and η_g is the gear efficiency, respectively. By way of example, using the specifications of Toyota Prius 2004 shown in Fig. 1*a* assuming that road inclination angle to be zero and the vehicle operation is in pure electric mode [3], the required traction machine torque and power over the NEDC can be derived in Fig. 1*b*. Based on maximum demanded torque, power, and speed of traction machine over NEDC extracted from Fig. 1*b*, maximum torque $T_{e(max)}$; continuous rated torque $T_{e(rated)}$; maximum speed $\omega_{e(max)}$; and base speed $\omega_{e(base)}$ of the employed traction machine can be defined assuming that a two-time short-period overload and an operated speed higher than five times of its base speed in the FW region. However, it is noted that the torque–speed characteristic can be also be defined by the powertrain developer. Using the obtained base and maximum speed, the number of pole pair n_p, machine slot n_{slt}, and air gap length l_g can be defined via a compromised selection based on dynamic balance, operating loss maps, and machine type (IPM, SPM…). Also, based on the selected machine type, PM material, and electrical steel material, air gap flux density value B_g together with core flux density B_c at the rated torque can be defined. It is noted that B_c value should be selected lower than the knee point value in the *B–H* curve, a factor associated with the required overload capability. Furthermore, relevant maximum current density J_m at the continuous rated torque can be determined based on utilised cooling method [6]. Moreover, the pole–arc angle α_{pa} can be defined for minimising the total harmonic distortion of IPM machine air gap flux density [1]. Illustration of IPM machine dimensions can be seen in Fig. 2, where l_m is the magnet length; l_g is the air gap length; s_{dpt} is the slot depth; s_{wg} is the slot wedge height; t_{dpt} is the tang depth; t_{op} is the tooth opening; t_{wd} is the

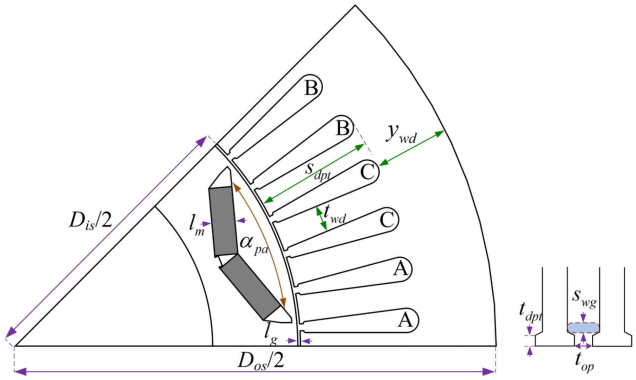

Fig. 2 *Geometries of studied IPM traction machine*

tooth width; and y_{wd} is the yoke width. It is noted that based on the number of tooth per pole, there is a relation factor k_{t2y} between tooth flux density $B_{c(t)}$ and the yoke flux density $B_{c(y)}$ with $B_{c(y)} = k_{t2y}B_{c(t)}$ [7].

According to [7], for given air gap and core flux densities, there is an optimum split factor $k_{of} = (D_{or}/D_{os})$ to achieve maximum torque per machine volume as shown in (3). On the other hand, it is well known that IPM machine torque is contributed by both the electromagnetic torque T_{em} shown in (4) with k_{w1} and k_{pk} is, respectively, the fundamental winding factor (relying on winding arrangement) and the slot packing factor (around 0.4–0.6) together with the reluctance torque T_{rlt} (discussed later in the next section). By assuming that each torque component equally contributes to the machine rated torque $T_{e(rated)}$ and the current angle β referred to the q-axis at this rated torque is approximated as around 40°–45° [2], (3) and (4) can be solved to derive the relationship between D_{or}, D_{os}, and l_{stk}

$$k_{of} = \left[(-3b_{of}/2) - \sqrt{(3b_{of}/2)^2 - 8a_{of}}\right]/(4a_{of}) \tag{3}$$

$$\begin{aligned} \text{where}\quad a_{of} &= \gamma^2 4\pi[\pi/(n_{slt}k_{t2y}) + 1]/(n_{slt}k_{t2y}) + 2\gamma - 1 \\ b_{of} &= -4\gamma\pi/(n_{slt}k_{t2y}) - 2\gamma \\ \gamma &= B_g/B_c \\ T_{em} &= \pi^2 k_{wl}k_{pk}B_g J_m D_{os}^2 l_{stk} D_{or} f_{of}/(16\sqrt{2}) \end{aligned} \tag{4}$$

$$\text{where}\quad f_{of} = a_{of}k_{of}^2 + b_{of}k_{of} + 1;$$

In addition, for the traction machine under consideration, its operation at base speed and continuous rated torque should maintain a specific efficiency e_{base} leading to (5) where the computation of copper loss P_{loss}^{cu} and core loss P_{loss}^{c} are expressed in (6) and (7), respectively:

$$P_{loss} = P_{loss}^{cu} + P_{loss}^{c} = (1 - e_{base})P_{base} \tag{5}$$

$$P_{loss}^{cu} = (\pi k_{pk}J_m^2\rho_{cu}f_{of}D_{os}^2/8)[2l_{stk} + D_{is}\pi^2/(2n_p)] \tag{6}$$

$$\text{where } D_{is} = D_{or} + 2l_g$$

$$P_{loss}^{c} = (\pi/4)(D_{os}^2 - D_{is}^2 - D_{os}^2 f_{of})l_{stk}\rho_c w_c(f, B_c) \tag{7}$$

where ρ_c is the core mass density (kg/m^3) and w_c is the manufacturer core loss data (W/kg) with core flux density and operating frequency f as its inputs, see Fig. 3.

Solving (3)–(7) results in common dimensions D_{or}, D_{is}, D_{os}, and l_{stk} for the required IPM traction machine to achieve a specific base speed, continuous rated torque, and relevant efficiency value.

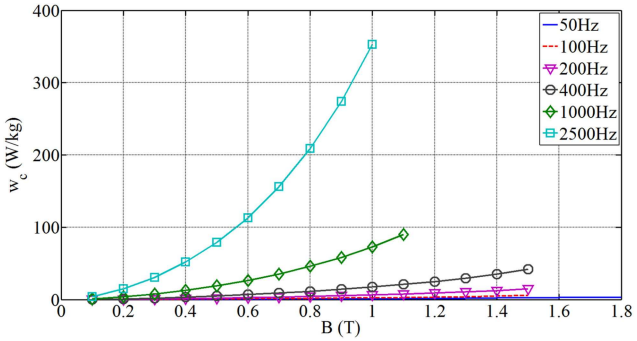

Fig. 3 *Manufacturer core loss data with operating frequency and flux density as its inputs, M270-35A*

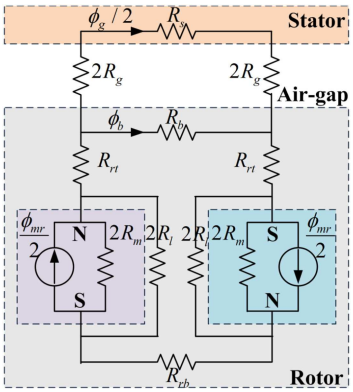

Fig. 4 *Equivalent lump parameter magnetic circuit of studied IPM traction machine [8]*

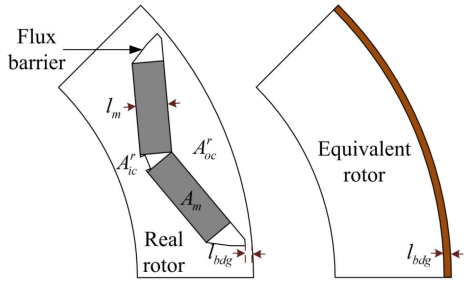

Fig. 5 *Actual rotor and equivalent outer ring for studying of centrifugal force*

2.2 Stator sizing

The stator sizing mainly focuses on computing stator geometries shown in Fig. 2 together with defining the maximum current I_{max}, the phase winding turn number n_t, and the relevant DC-link voltage V_{dc}. First, the tooth width and yoke width can be derived via the relationship between tooth flux density $B_{c(t)}$, yoke flux density $B_{c(y)}$, and air gap flux density in (8) and (9), respectively.

$$B_{c(t)} = B_g \pi D_{is}/(n_{slt} t_{wd}) \tag{8}$$

$$B_{c(y)} = B_g D_{is}/(2 n_p y_{wd}) \tag{9}$$

Using the obtained y_{wd} and t_{wd}, relevant tooth depth value can be derived as

$$t_{dpt} = [(D_{os} - D_{is})/2] - y_{wd} \tag{10}$$

The tooth opening t_{op} can be selected as two times of coil strain diameter for manufacturing purpose. The tang depth t_{dpt} value can be selected to be equal to t_{op}. The slot wedge s_{wg} height depends on the employed slot wedge material.

As aforementioned, the total torque of the IPM machine is contributed by T_{em} and T_{rlt} (11). In (12), the relationships between T_{em}, I_m, and n_t are presented. In addition, by defining a saliency factor ξ between d- and q-axis magnetising inductance (13), relevant relationship between T_{rlt} and I_m together with n_t can be derived in (14) where $l_{g(q)}^{eqv}$ is the equivalent air gap in the q-axis considering leaking and fringing effects. This equivalent air gap can be approximated with a given leaking and fringing factor. By assuming an equal contribution of electromagnetic torque and reluctant torque to the machine rated torque together with setting relevant current angle β around 40°–45° [2], (11)–(14) can be solved to derive I_m and n_t. Based on the obtained n_t, stator resistance r_s and leakage inductance L_{lk} can be computed [6]. For a two-time short-period overload capability, the maximum current of the studied IPM traction machine neglecting saturation effect I_{max} can be considered as $2I_m$

$$T_e = T_{em} + T_{rlt} \tag{11}$$

$$T_{em} = 3 n_p I_m \psi_m \cos(\beta)/2; \quad \psi_m = k_{w1} n_t B_{g1} D_{is} l_{stk}/n_p \tag{12}$$

$$\xi L_{md} = L_{mq}; \quad L_{mq} = 3\mu_0 \pi D_{is} l_{stk} (k_{w1} n_t)^2/(8 l_{g(q)}^{eqv} n_p^2) \tag{13}$$

$$T_{rlt} = 3 n_p (\xi - 1) L_{mq} I_m^2 \sin(2\beta)/(4\xi) \tag{14}$$

In practice, as traction machine in the EV will be driven via a battery pack in the electric operating mode, the DC link voltage value V_{dc} can be determined in advance considering current and voltage limitations associated with the employed battery pack. However, a minimum V_{dc} required to balance machine voltage at base speed and peak torque can be determined using (15), where k_{mi} is the maximum modulation index of the employed machine drive [2] and v_m is the machine voltage associated with the total air gap flux density. The current angle β at that peak torque still can be selected from 40°–45°.

$$V_{dc} k_{mi} - r_s I_{max} \geq v_m \tag{15}$$

where

$$\psi_d = -I_{max} \sin(\beta)(L_{lk} + L_{md}) + \psi_m$$

$$\psi_q = I_{max} \cos(\beta)(L_{lk} + L_{mq})$$

$$v_m = \omega_{e(base)} \sqrt{\psi_d^2 + \psi_q^2}$$

2.3 Rotor sizing

The purpose of the rotor sizing step is to define appropriate magnet length l_m to provide the air gap flux B_g, ensure demagnetising protection, and maintain the saliency factor ξ for a given reluctance torque achievement. According to [8], equivalent plump parameter magnetic circuit of one-half machine pole pair is illustrated in Fig. 4, where R_s, R_g, R_b, R_{rt}, R_l, and R_{rb} are the stator reluctance, air gap reluctance, rotor bridge reluctance, rotor section on top PM reluctance, rotor flux barrier reluctance, and rotor section on bottom PM reluctance, respectively, see Fig. 5. Using this circuit, the air gap flux density can be expressed in (16), where k_{lkg} is the total leakage factor, k_{rlt} is the reluctance factor, μ_{mr} and B_{mr} are the relative permeability and remanent flux density of the selected PM material, respectively. Details of magnetic circuit analysis and computing of k_{lkg} and k_{rlt} can be found in [8]

$$B_g = k_{lkg} B_{mr} (\alpha_{pa}/\pi)/[1 + (k_{rlt} k_{lkg} \mu_{mr} l_{g(d)}^{eqv}/l_m)] \tag{16}$$

On the other hand, the magnet length should also be selected to avoid demagnetising when I_{max} is applied in the opposite direction of PM flux as shown in (17), where B_{mr}^{kn} corresponds to value at the knee point in B–H curve of the selected PM material

$$B_g - B_{mr}^{kn} \geq 3 k_{w1} \mu_0 n_t I_{max}/(\pi n_p l_{g(d)}^{eqv}) \tag{17}$$

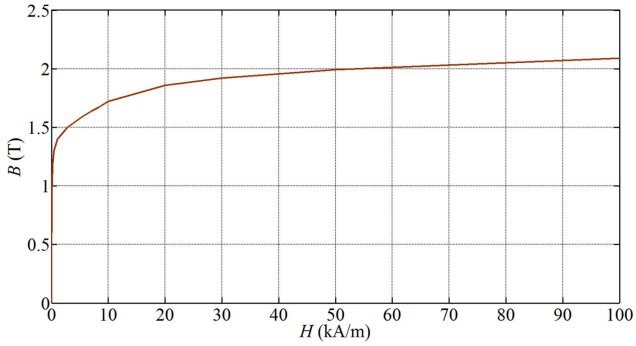

Fig. 6 *B–H curve of selected electrical steel (M270-35A)*

Rearranging (17), relevant $l_{\rm m}$ value can be obtained via solving (18)

$$a_{\rm lm} l_m^2 + b_{\rm lm} l_m + c_{\rm lm} = 0 \tag{18}$$

where

$$a_{\rm lm} = f_{\rm lm1} - B_{\rm mr}^{\rm kn}$$

$$b_{\rm lm} = \mu_{\rm mr}(f_{\rm lm1} l_g - f_{\rm lm3}) - B_{\rm mr}^{\rm kn}(f_{\rm lm2} - \mu_{\rm mr} l_{g(d)}^{\rm eqv})$$

$$c_{\rm lm} = -\mu_{\rm mr} f_{\rm lm2}(f_{\rm lm3} + B_{\rm mr}^{\rm kn} l_g)$$

$$f_{\rm lm1} = k_{\rm lkg} B_{\rm mr}$$

$$f_{\rm lm2} = k_{\rm rlt} k_{\rm lkg} \mu_{\rm mr} l_g \alpha_{\rm pa}/\pi$$

$$f_{\rm lm3} = \sqrt{2}\mu_0 k_{\rm wl} J_m k_{\rm pk} D_{\rm os}^2 f_{\rm of}/(8 n_p)$$

In addition, the magnet length also should be determined to maintain a specific saliency value for a specific reluctance torque achievement. According to [6, 9], *d*- and *q*-axis inductance of the IPM machine can be computed using (19) and (20), where $P_{\rm m}$ is the effective magnet permeance associated with $l_{\rm m}$

$$L_d = L_{\rm lk} + L_{\rm md} = L_{\rm lk} + 3L_{{\rm slf}(d)} k_{\alpha d}/2 \tag{19}$$

$$L_q = L_{\rm lk} + L_{\rm mq} = L_{\rm lk} + 3L_{{\rm slf}(q)} k_{\alpha q}/2 \tag{20}$$

$$\text{where } k_{\alpha d} = 1 - \frac{(4/\pi)\sin(\alpha_{\rm pa}^{\rm pu}\pi/2)[\alpha_{\rm pa}^{\rm pu} + \sin(\alpha_{\rm pa}^{\rm pu}\pi)/\pi]}{(1 + P_m R_g)}$$

$$k_{\alpha q} = \alpha_{\rm pa}^{\rm pu} - [\sin(\alpha_{\rm pa}^{\rm pu}\pi)/\pi]$$

After solving (16), (18)–(20), $l_{\rm m}$ is selected as the maximum value obtained.

On the other hand, the bridge length of an IPM machine rotor should be chosen to withstand its own centrifugal force and that of the inner magnets, see Fig. 5. According to [4], by defining an equivalent outer ring area $A_{\rm eqv}$ with similar minimum bridge length $l_{\rm bdg}$ and an equivalent mass density $\rho_{\rm eqv}$ represented for the bridge area associated with the covering outer rotor core area and $A_{\rm oc}^r$ the magnet area $A_{\rm m}$ shown in Fig. 5 (21), the new equivalent outer ring must withstand the original centrifugal force as shown in (22), where $\sigma_{\rm t(eqv)}$ is the equivalent tangential stress, $k_{\rm ovs}$ is the over speed factor, and $\sigma_{\rm t(max)}$ is maximum yield strength of selected electrical steel material

$$\rho_{\rm eqv} = \rho_c(A_{\Sigma m} + A_{\Sigma oc}^r)/A_{\rm eqv} \tag{21}$$

$$\sigma_{\rm t(eqv)} = (D_{\rm or} - l_{\rm bdg})^2 \omega_{\rm max}^2 k_{\rm ovs}^2 \rho_{\rm eqv}/4 = \sigma_{\rm t(max)}/2 \tag{22}$$

2.4 Consideration of saturation effects on material

After all machine dimensions have been determined, machine parameters including stator resistance, *dq*-axis inductance (19) and (20), and PM flux linkage (12) will be calculated using the obtained geometry values. It is noted that the IPM machine is well known for its non-linear characteristics due to its small air gap length. Thus, the iterative process introduced in [5] is utilised using *B–H* curve of the selected material, see Fig. 6, to analyse the saturation effects in the studied machine characteristics.

3 Validation of proposed concept

The proposed method is validated using Toyota Prius 2004 specifications [3] over the New European Driving Cycle (NEDC), see Fig. 1, with measurements taken from [10] as a benchmark. M270-35A and NdFeB (N4025) are, respectively, selected for electrical steel and PM materials. By assuming during the NEDC driving cycle, the studied vehicle is driven by an IPM machine of which both electromagnetic torque and reluctance torque equally contributes to its rated torque at base speed with around 90% efficiency achievement, machine geometries, parameters considering material saturation effects, and operating efficiency maps can be generated within seconds using the proposed sizing method. For a given torque–speed operating point, machine core loss, copper loss, and efficiency can be computed via (23)–(25). Relevant *dq*-axis currents at a given torque–speed operating point shown in (24) are calculated via the control method presented in [2, 3]

$$P_{\rm loss}^{\rm c} = w_{\rm c}(f, B_{\rm c}) m_{\rm c}^{\rm s} = w_{\rm c}^{\rm t}(f, B_{{\rm c}(t)}) m_{{\rm c}(t)}^{\rm s} + w_{\rm c}^{y}(f, B_{{\rm c}(y)}) m_{{\rm c}(y)}^{\rm s} \tag{23}$$

where $m_{\rm c}^{\rm s}$ is the stator core mass; $m_{\rm c(t)}^{\rm s}$ is the stator core tooth mass; and $m_{c(y)}^{s}$ is the stator core yoke mass

$$P_{\rm loss}^{\rm cu} = 3(i_d^2 + i_q^2) r_s/2 \tag{24}$$

$$e = [T_{\rm e}\omega_{\rm m}/(T_{\rm e}\omega_{\rm m} + P_{\rm loss}^{\rm cu} + P_{\rm loss}^{\rm c})] \tag{25}$$

Main geometries of the MG2 Toyota Prius 2004 traction machine [10] and the proposed technique results are presented in Table 1, where it is shown that there is a good match in sizing between the proposed method and the MG2 (maximum 4% difference for stator resistance). To further verify the proposed technique, FE package is employed to analyse the studied IPM machine characteristics using obtained machine geometries from the proposed method. Fig. 7 shows well-matched results between the proposed technique and the FE study. In Fig. 8, torque waveform at the continuous rated value (200 N m) and the peak value (400 N m) under FE study are also presented with relevant current angle β as 47° and 48°, respectively. Using these values, it can be demonstrated that the electromagnetic torque considering saturation effect, respectively, contributes up to 64% and 45% of the rated and peak torque of the studied IPM traction machine torque. In addition, no-load loss (core loss) from the proposed method is also well validated with both FE and measured results [10], see Fig. 9.

In Fig. 10, well-matched current magnitude between the proposed technique, see Fig. 10*a*, and measurement [10], see Fig. 10*b*, over the speed–torque operating range can be observed. By comparison machine efficiency maps between the proposed technique in Fig. 11*a* and measurement [10] in Fig. 11*b*, the efficiency of the proposed rapid sizing method can be highly demonstrated. It is noted that with a limited computing resource, it is only taken <1 min for the proposed technique to complete the

Table 1 Comparison between the proposed concept results and MG2 Toyota Prius 2004 [10]

Specifications	MG2 Toyota	Proposed concept	Diff., %
power, W	50,000	50,552	1.104
maximum speed, rpm	6000	5994.5	0.917
peak torque, Nm	400	402.65	0.6625
D_{os}, mm	269	270.42	0.5278
D_{is}, mm	161.9	160.33	0.9697
D_{or}, mm	160.5	158.9	0.9968
V_m, cm^3	163.2	163.41	0.1286
l_{stk}, mm	84	83.78	0.261
number of turns	72	72	0
r_s, Ω	0.069	0.066	4.348

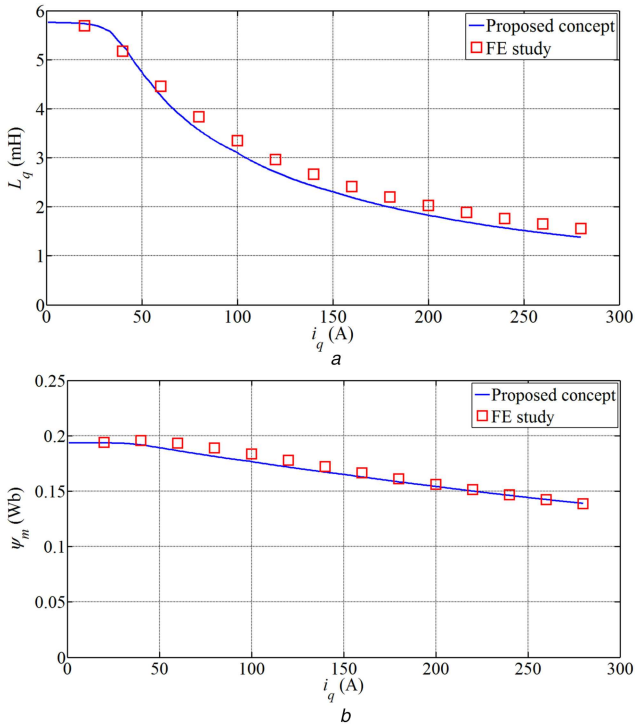

Fig. 7 *Machine parameters considering saturation effects.*
(a) *q*-axis inductance. ***(b)*** PM flux linkage

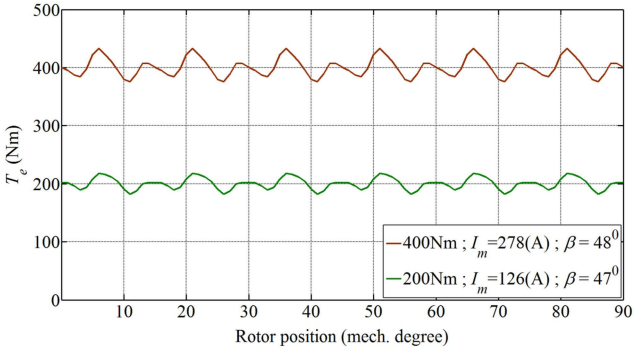

Fig. 8 *Torque waveform and relevant current magnitude at rated torque and peak torque demand from FE study*

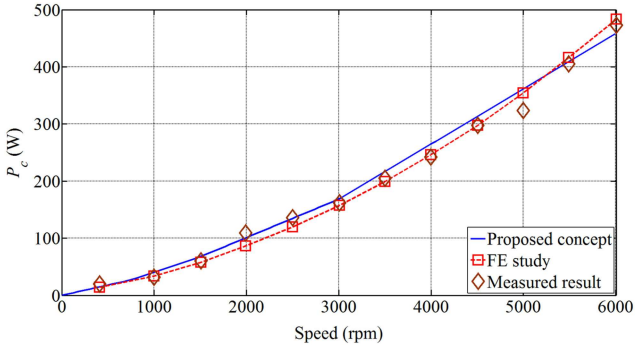

Fig. 9 *Comparative no-load loss results of the proposed concept, FE, and measurement [10]*

sizing (Table 1), compute machine parameters considering saturation effects (Fig. 7), and generate relevant operating and efficiency maps [shown in Figs. 10*a* and 11*a*].

4 Conclusion

This paper presents a rapid sizing method for IPM traction machine considering saturation effects. It has been demonstrated that with limited computing resources, sizing, parameters considering saturation effects, and efficiency maps of an IPM machine can be generated and the efficiency of the machine can be estimated over the NEDC cycle, e.g. within seconds with acceptable accurateness in comparison with FE study and measured results. The proposed rapid sizing method is highly essential at the preliminary design stage of EV powertrains.

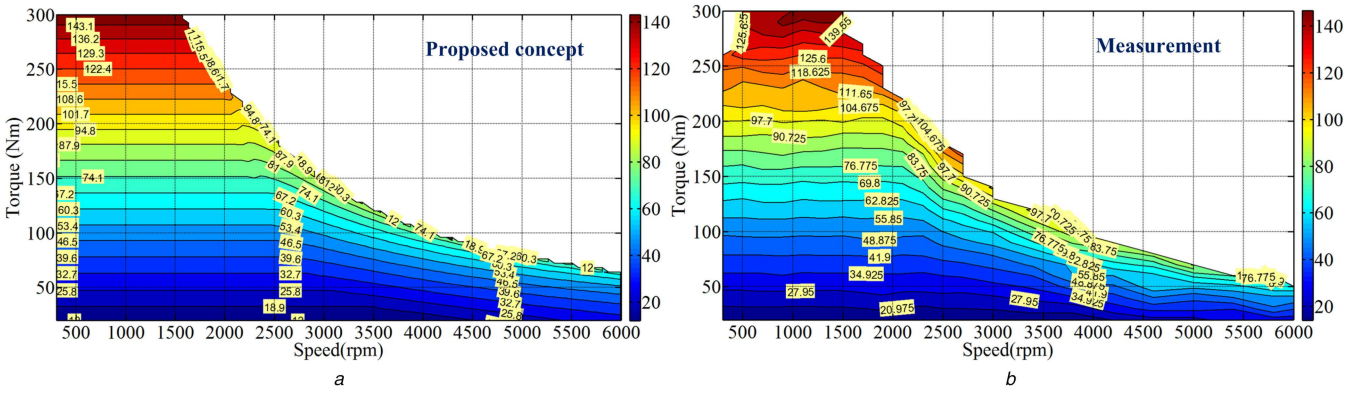

Fig. 10 *Phase current in RMS over speed and torque range.*
(a) Proposed concept. ***(b)*** Measured result [10]

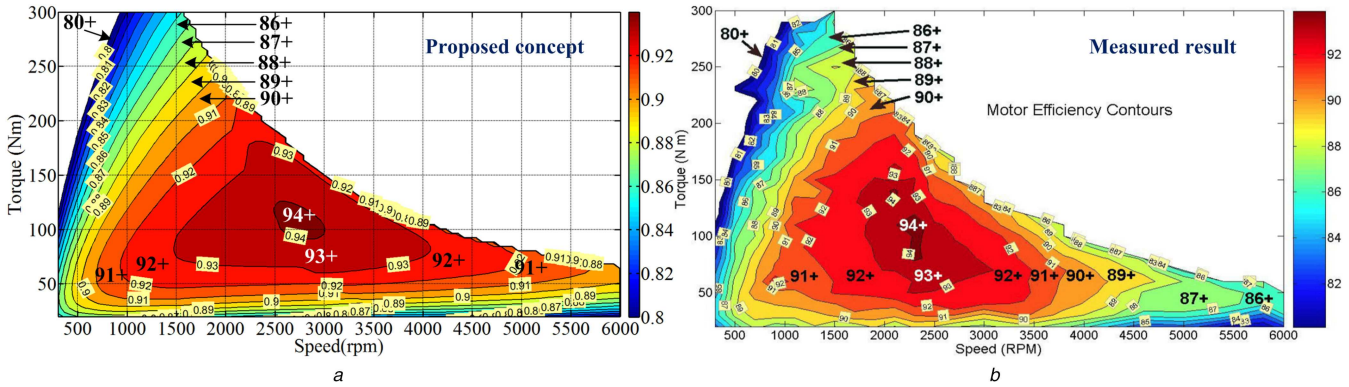

Fig. 11 *IPM traction machine efficiency over speed and torque range.*
(a) Proposed concept. ***(b)*** Measured result [10]

5 References

[1] Kamiya, M.: ‘‘Development of traction drive motors for the Toyota hybrid systems’, *IEEJ Trans. Ind. Appl.*, 2006, **126**, (4), pp. 473–479

[2] Hoang, K. D., Aorith, H.: ‘Online control of IPMSM drives for traction applications considering machine parameter and inverter nonlinearities’, *IEEE Trans. Transp. Electrification*, 2015, **1**, (4), pp. 312–325

[3] Hoang, K. D., Atallah, K.: ‘A rapid concept development technique for electric vehicle power trains’. Proc. IEEE Int. Conf. Connected Vehicles and Export (ICCVE) 2014, Vienna, Austria, Nov. 3–7, 2014, pp. 191–198

[4] Binder, A., Schneider, T., Klohr, M.: ‘‘Fixation of buried and surface mounted magnets in high-speed permanent-magnet synchronous machines’, *IEEE Trans. Ind. Appl.*, 2006, **42**, (4), pp. 1031–1037

[5] Hsieh, M.F., Hsu, Y.-C.: ‘A generalized magnetic circuit modelling approach for design of surface permanent-magnet machines’, *IEEE Trans. Ind. Electron.*, 2012, **59**, (2), pp. 779–792

[6] Hendershot, J. R., Miller, T. J. E.: ‘*Design of brushless permanent magnet machine*’ (Motor Design Books LLC, Venice, FL, USA, 2010)

[7] Pang, Y., Zhu, Z. Q., Howe, D.: ‘Analytical determination of optimal split ratio for permanent magnet brushless motors’. *IEE Proc. – Electric Power Applications*, 2006, **153**, (1), pp. 7–13

[8] Hanselma, D.: ‘*Brushless motors: magnetic design, performance, and control*’ (E-Man Press LLC, New York, NY, USA, 2012)

[9] Gieras, J.F., Santini, E., Wing, M.: ‘‘Calculation of synchronous reactances of small permanent-magnet alternating-current motors: comparison of analytical approach and finite element method with measurement’, *IEEE Trans. Magn.*, 1998, **34**, (5), pp. 3712–3720

[10] Staunton, R. H., Ayers, C. W., Chiasson, J. N., *et al.*: ‘Evaluation of 2004 Toyota Prius hybrid electric drive system’. Tech. Rep. ORNL/TM- 2006/423, Oak Ridge Nat. Lab., Oak Ridge, TN, 2006